Atmospheric Environment 146 (2016) 332–345

Contents lists available at ScienceDirect

Atmospheric Environment

journal homepage: www.elsevier.com/locate/atmosenv

Acid rain attack on outdoor sculpture in perspective

Richard A. Livingston

Materials Science & Engineering Dept., U. of Maryland, College Park, MD 20742, USA

HIGHLIGHTS

- Most significant sculptural materials are carbonate stone and bronze.
- Weathering processes due to rain can be measured by the mass balance method.
- Geochemical modeling can be applied to analyze mass balance data.
- Rain acidity effects are negligible compared to dry deposition.
- Organic acids may also have a significant effect.

ARTICLE INFO

Article history:
Received 29 February 2016
Received in revised form
3 July 2016
Accepted 8 August 2016
Available online 9 August 2016

Keywords:
Acid rain
Dry deposition
Bronze
Marble
Sea salt
Organic acids

ABSTRACT

A major concern motivating research in acid rain materials effects has been the potential for damage to cultural heritage, particularly outdoor marble and bronze sculpture. However, a combination of field and laboratory studies has failed to show a correlation between rain pH and loss of materials. In order to understand this counterintuitive lack of acid rain effect, an aqueous geochemical modeling approach was used to analyze rain runoff chemistry for the relative importance of acid rain neutralization, dry deposition, and in the case of marble, natural carbonate dissolution. This approach involved the development of pH – SO_4^{2-} phase diagrams for marble (calcium carbonate) and bronze (copper) under ambient environmental conditions. This then enabled reaction path modeling of the acid neutralization process using the pH range typically found in wet deposition (3.5–6). The results were for marble that the theoretical maximum amount of Ca^{2+} ion that could be lost due acid rain neutralization would be 0.158 mmol/l compared to 10.5 mmol/l by dry deposition, and for bronze, the Cu^{2+} ion losses would be 0.21 mmol/l and 47.3 mmol/l respectively. Consequently dry deposition effects on these materials have the potential to dominate over wet deposition effects. To test these predictions the geochemical models were applied to examples of data sets from mass balance (runoff vs rainfall) studies on a marble statue in New York City and some bronze memorial plaques at Gettysburg PA. Although these data sets were collected in the early 1980s they remain valid for demonstrating the mass balance method. For the marble statue, the mean Ca^{2+} losses by dry deposition was about 69% of the total compared 0.3% for acid rain neutralization, which was less than the natural carbonate dissolution losses of 0.8%. For the bronze, the mean Cu^{2+} losses were 70.6% by SO_4^{2-} dry deposition and 23% by NO_3^- dry deposition compared to 6.4% by acid rain neutralization. Thus for both cases the wet deposition component was less than the variability of the dry deposition components, which explains the observed lack of correlation between the rain pH and the material losses. In addition, for the marble case, there was evidence for HCl acid vapor attack resulting from nitric acid/sea salt interactions and for bronze, ammonium ion may be important. In both cases, significant imbalances suggested that unmeasured organic acids may have a significant effect.

1. Introduction

During the 1970s and 1980s, public concern about acid rain effects often focused on its potential damage to outdoor works of art, which includes both sculptural details on buildings and free standing statues. In fact one eminent scientist in the field of stone conservation predicted in 1973 that the loss of cultural heritage would increase exponentially by the end of the millennium (Winkler, 1973). However, after over a decade of research, it was

E-mail address: rliving1@umd.edu.

http://dx.doi.org/10.1016/j.atmosenv.2016.08.029

concluded that for marble and bronze, the two materials most often used for outdoor sculpture, the effect of acid rain was negligible (Meakin et al., 1992; Mossotti et al., 2001). In order to understand this counterintuitive result, geochemical reaction path models have been developed that make it possible to investigate the contributions of the individual processes that are involved in the weathering of these materials.

Outdoor sculpture has traditionally been made from two major groups of inorganic materials: stone and metals. A rough idea of the relative frequency of occurrence of these materials in outdoor sculpture in the United States is given by Table 1, which has been compiled from a data base that is maintained by the American Art Museum of the Smithsonian Institution (Smithsonian American Art Museum, 2015).

Although many different types of stone have been used for sculpture, the most vulnerable to potential acid rain damage are marble and limestone (Steiger, 2015). The former is essentially a recrystallized form of the latter; both are composed of calcite ($CaCO_3$). Other types of stone which are composed of silicate minerals such as granite or sandstone are intrinsically more resistant to acid attack.

A variety of metals have been used in sculpture including cast iron, steel, zinc and lead and bronze. Tidblad (2015) has made a recent review of the literature on air pollution effects on metals. Bronze has been preferred for sculpture since antiquity because of its resistance to corrosion and favorable casting properties. As indicated in Table 1, it is by far the most widely used metal in sculpture in the United States.

The term “bronze” actually covers a wide range of compositions in the quaternary system Cu-Zn-Sn-Pb. Pure copper is too soft for practical applications. Consequently, other elements have usually been added to harden it and possibly also to change its color. These has varied over time as shown in Table 2. In antiquity, tin was the major alloying element, despite its high cost. Small amounts of lead improve the flowability of the molten bronze and enhance its ability to reproduce fine details. Since the Renaissance the trend has been to replace tin with lower cost zinc. Since the 19th century sculptural bronze has contained 85–95% copper (Selwyn, 1996). The term “architectural bronze” is currently in wide use for a 57% Cu 40% Zn 3% Pb composition, although technically a copper alloy with this level of zinc should be called brass (CDA, 2015).

The total erosion rate of a material exposed to the outdoor environment consists of two components: chemical dissolution and granular disintegration. The latter consists of the loss of solid grains of the material due to mechanical forces of gravity, wind, thermal cycling etc. Chemical dissolution often facilitates granular disintegration by attacking the intergranular binding phases that hold the grains together.

The three metrics of erosion rates are: surface recession, weight loss or solution mass balance. Their features are compared in Table 2. Surface recession is measured in terms of the displacement of a point on the current surface from a reference point representing the original position of the surface. This usually done using a micrometer depth gauge mounted in a frame attached to some bolts or studs that are permanently installed in the surface (Stephenson and Finlayson, 2009). Mass loss is the method typically used for measuring atmospheric corrosion of metals. It consists of measuring the weight change of tablets or coupons of material after exposure to the atmosphere (ASTM, 2011). Finally, the mass balance method consists of collecting rain water falling on the surface and simultaneously collecting the runoff. The difference in solution chemistry is the result of reactions taking place with the material (Livingston, 1986). The magnitude of the attack is estimated by the increase in the concentration of a characteristic cation that is representative of the material, Ca^{2+} in the case of carbonate stone and Cu^{2+} for bronze.

The three metrics are incommensurate, strictly speaking, since each concerns a different type of dimension: distance for surface recession, mass for mass loss and concentration for mass balance. It is possible to make some approximate conversions from one metric to another using various assumptions. For example, with knowledge of the sample's surface area and material density, a mass loss measurement can be converted into a penetration depth which approximates an average surface recession. However, the uncertainties in the calculated penetration depth can be significant in the case of a granular and porous material such as limestone.

As shown in Table 2, both surface recession and mass loss measure the total erosion rate, but cannot distinguish between granular disintegration and chemical dissolution. Moreover, they cannot resolve acid deposition attack into its wet and dry deposition components. On the other hand, the mass balance measurement can discriminate explicitly between acid rain damage and other types of damage using geochemical modeling as described in Section 2. However, since it measures only chemical dissolution, it can't give an estimate of total erosion rate.

Finally, micro-erosion meter measurements are difficult to apply to outdoor sculpture because a horizontal planar surface is required. Moreover, it involves installing a set of studs into the surface, which could be objectionable on esthetics grounds. Similarly, mass loss measurements are not practical for outdoor sculpture which typically consists relatively massive objects permanently fixed in place. Only the solution mass balance approach, which is nondestructive and can be applied to irregularly shaped objects, is feasible.

The mass balance method provides data consisting of concentrations of ions. To order to extract useful information from these data, it is necessary to apply geochemical modeling techniques. In the following sections, geochemical models for the attack of acidic

Table 1
Occurrence of outdoor sculptural materials in the United States (number of entries).

Stone		Metal	
Marble	4483	Bronze	13,151
Limestone	2048	Steel	7270
Sandstone	597	Aluminum	1400
Granite	8668	Cast iron	462
		Zinc	188
		Lead	131

Table 2
Comparison of damage quantification metrics.

	Surface recession	Mass loss	Solution mass balance
Measurement method	Micro-erosion meter	Gravimetry	Rainfall/runoff difference
Erosion processes	Chemical dissolution + granular disintegration	Chemical dissolution + granular disintegration	Chemical dissolution
Acid deposition components	No	No	Yes
Precision	5 μm	10 μg	1 μg/l
Dimensionality	Point	Volume	Area
Applicable to sculpture	No	No	Yes

deposition on carbonate stone and bronze are developed. They are then applied to case studies of a marble statue in New York City and a set of bronze memorial plaques at Gettysburg, PA.

2. Geochemical models

This approach makes use of the principles of aqueous geochemistry to develop phase diagrams that predict which solid phases are stable in contact with solutions of a given pH and chemical composition (Stumm and Morgan, 1981). The diagrams can then be used to visualize the reactions paths followed by solutions such as acid rain to approach equilibrium through different processes such acid rain neutralization, dissolution of dry deposition reaction products or other non-acidic deposition effects. The characteristic changes in the anions and in pH along each reaction path can be used to quantify the relative importance of the individual processes.

2.1. Carbonate stone

2.1.1. Acid deposition

Wet deposition, or acid rain, is defined as the presence of acidity in rainwater in excess of naturally occurring acids as a result of human activities. This anthropogenic contribution consists mainly of sulfuric acid with lesser and more variable amounts of nitric acid. Contact of such a solution with carbonate stone neutralizes this acidity through the reaction:

$$CaCO_3 + 2H^+ + SO_4^{2-} \rightarrow Ca^{2+} + H_2O + CO_2\uparrow + SO_4^{2-} \quad (1)$$

This has been written in a redundant fashion to emphasize that it does not produce a net change in the concentration of SO_4^{2-}. The same would hold true for NO_3^- or any other acidic anion present. Hence, it does not matter whether the acid component of the rain is purely sulfuric or a mixture of sulfuric and nitric acids. The only effect of this reaction on the mass balance is thus the reduction of H^+, or the equivalent increase in pH.

Dry deposition takes place in the intervals between precipitation events. Sulfur bearing acidic gases or particulate matter react with the carbonate stone surface in various ways to produce gypsum ($CaSO_4 \cdot 2H_2O$) which has a much greater solubility than calcite, 2 g/l and 43 mg/l respectively. This mineral then dissolves in runoff:

$$CaSO_4 \cdot 2H_2O \rightarrow Ca^{2+} + SO_4^{2-} + 2H_2O \quad (2)$$

Since this reaction involves only the dissolution of a neutral salt, there is no shift in pH or carbonate species concentrations, but there is a net gain in SO_4^{2-} concentration, which is therefore the signature for gypsum dissolution, and by inference dry deposition. There is also the possibility of NO_x or HNO_3 gas deposition, with the subsequent formation of calcium nitrate salts, but there is little direct field evidence to support this (Steiger, 2015).

2.1.2. Karst effect

Even in the absence of any anthropogenic acidity, carbonate stone will dissolve in rainwater, since calcite has a slight solubility in pure water, which is theoretically 11 mg/l at 25 °C. This is enhanced in the presence of atmospheric carbon dioxide, and at the atmospheric CO_2 pressure of 101.5 Pa ($10^{-3.5}$ bar), it reaches 43 mg/l (Butler, 1982). This slight amount of dissolution becomes very significant over geological time periods and produces characteristic caverns and mountain peaks in limestone formations that are usually classified under the heading of karst landforms (Ford and Williams, 2007). This naturally-occurring dissolution process, referred to from now on as the karst effect, is given by the overall equation:

$$CaCO_3 + H_2O + CO_2 \rightarrow Ca^{2+} + 2HCO_3^- \quad (3)$$

The bicarbonate, HCO_3^-, ion concentration is determined by the relationship:

$$\left\{HCO_3^-\right\} = \frac{10^{-7.82} P_{CO_2}}{\{H^+\}} \quad (4)$$

where the curly brackets indicate activities. However, the ionic strengths of rainfall and runoff solutions are typically low enough that the activity coefficients all approach unity, and thus molarities can be used as an approximation for activities. Inserting the value of atmospheric P_{CO2} in Eqn. (4) gives:

$$HCO_3^- = \frac{10^{-11.32}}{H^+} \quad (5)$$

This implies that in the case of pristine rainwater, which in theory has no acidic species other than carbonate ion, Eqn (5) has a fixed pH of 5.65. Therefore, only rain that has a pH lower than this value can be classified as true anthropogenic acid rain.

2.1.3. The three-component model

The observed increase in Ca^{2+} is thus the sum of three different reactions, each representing a different weathering process and which produces its own unique combination of changes in concentrations of the anions SO_4^{2-}, H^+ and HCO_3^-. Applying the electroneutrality condition, the total difference in solution chemistry between runoff and rainfall of these three processes can be written as:

$$\Delta Ca^{2+} = 0.5\Delta HCO_3^- - 0.5\Delta H^+ + \Delta SO_4^{2-} \quad (6)$$

where Δ is the difference operator $x_{\text{runoff}} - x_{\text{rainfall}}$, and the x values are molarities.

Furthermore, it is possible using the carbonate equilibria and the definition of acid rain to partition the total difference, ΔCa_T, into three linearly independent components:

$$\Delta Ca_T^{2+} = \Delta Ca_{ar}^{2+} + \Delta Ca_{dd}^{2+} + \Delta Ca_{ks}^{2+} \quad (7)$$

where subscripts are: ar = acid rain; dd = dry deposition and ks = karst.

Moreover, carbonate alkalinity is defined as:

$$Alk = HCO_3^- + 2CO_3^{2-} + OH^- - H^+ \quad (8)$$

However, in the pH range under consideration, CO_3^{2-} and OH^- are negligible, and hence Eqn. (8) reduces to:

$$Alk = HCO_3^- - H^+ \quad (9)$$

The alkalinity function has several convenient properties. It is zero at pH = 5.65, negative values indicate the presence of non-carbonate acidic species and positive values indicate increased carbonate species. Since acid rain neutralization concerns only the change of pH from the rain value to 5.65 and the karst effect only the change in pH from 5.65 to the runoff value, the two components can be written in terms of the alkalinity function as:

$$\Delta Ca_{ar}^{2+} = -0.5\Delta \text{Alk}_{rn} \quad (10)$$

And:

$$\Delta Ca^{2+}_{ks} = 0.5\Delta \mathrm{Alk}_{rf} \quad (11)$$

where the subscripts are: *rn* = rain and *rf* = runoff.

Finally, the dry deposition component is given by:

$$\Delta Ca^{2+}_{dd} = \Delta SO^{2-}_4 \quad (12)$$

Substituting Equations (10)–(12) into Eqn. (7) gives:

$$\Delta Ca^{2+} = 0.5Alk_{rf} - 0.5Alk_{rn} + \Delta SO^{2-}_4 = 0.5\Delta Alk + \Delta SO^{2-}_4 \quad (13)$$

As shown in the next section, the two variables *Alk* and SO^{2-}_4 can serve as the axes for constructing a phase diagram that can be used to visualize the carbonate stone attack.

Cardell-Fernandez et al. (2002) have criticized this three component model as the basis of a predictive model for stone damage on the grounds that it requires actual rain and runoff chemistry data. However, it is not intended to make predictions, but rather to serve as a method for the statistical analysis of field data in order to determine the relative importance of the various mechanisms causing stone damage.

2.1.4. Carbonate/acid rain phase diagram

The relationships among the three components can be visualized with aid of a suitable phase diagram (Fig. 1) which has a horizontal axis of SO^{2-}_4 molarity and a vertical axis of alkalinity. This displays the field of stability of calcite versus gypsum and a solution containing sulfuric acid. In reality, the solvus, i.e. the boundaries between solid phases and solution, consists of a 3-dimensional volume, with Ca^{2+} as the third axis. However this is difficult to visualize.

In the specific case of acid rain attack on carbonate stone this can be collapsed into a 2-dimensional diagram. Since the incident rainwater is nearly pure water, the resulting chemistry of the solution after contact with the stone is dominated by reaction with its mineral assemblage. Hence the electroneutrality condition can be approximated by:

$$Ca^{2+} = 0.5Alk + SO^{2-}_4 \quad (14)$$

This relationship can then be used to eliminate the variable Ca^{2+} in the solubility products of calcite and gypsum. Equation (14) defines a plane, and the phase diagram in Fig. 1 is thus the 2-dimensional result of the intersection of this plane with the volume of the solvus.

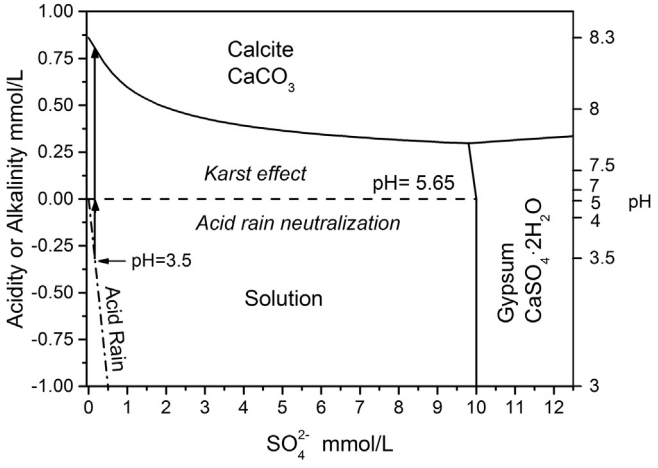

Fig. 1. Carbonate stone/acid rain phase diagram.

The use of this diagram to visualize the reaction paths of rainwater coming into contact with the stone is illustrated by the example shown in Fig. 1, which is the case of acid rain contacting carbonate stone in the absence of any dry deposition sulfate on the surface. The dash dot line in the diagram represents the composition of dilute sulfuric acid at different molarities. The lowest pH value that has been observed in rainwater in N. America is roughly 3.5 (NADP, 2014). Therefore, the start of the reaction path is at the point indicated on this line at that pH, which has a negative alkalinity of −0.36 mmol/l. As the acid is neutralized through the reaction of Eqn. (1), the solution composition changes in a direction parallel to the vertical axis, as shown by the lower arrow. When the solution composition reaches *Alk* = 0, indicated by the horizontal dashed line, all the incident acidity has been consumed. At that point the karst reaction of Eqn. (3) takes over, increasing the alkalinity of the solution, also in a direction parallel to the vertical axis as shown by the upper arrow. Eventually the solution alkalinity reaches the solvus line for calcite at the point marked by the head of the arrow which indicates that equilibrium has been achieved, and the karst reaction terminates.

According to Eqn. (10) the increase in Ca^{2+} is half the total increase in *Alk*, which is given by the sum of the lengths of the arrows as 1.123 mmol/l. Thus $\Delta Ca^{2+} = 0.5615$ mmol/l. However, the individual lengths of the lower and upper arrows are 0.316 and 0.807 mmol/l respectively. Consequently $\Delta Ca^{2+}_{ar} = 0.158$ mmol/l and $\Delta Ca^{2+}_{ks} = 0.404$ mmol/l. In other words, the karst effect accounts for 72% of the total carbonate dissolution and acid rain neutralization only 28%. Note that this is for the worst case, i.e. the lowest historically observed pH in incident rain. For higher pH rain, the starting point moves upward on the acid rain line, reducing the length of the path in the acid rain neutralization region of the diagram while the length of the path in the karst region increases because of the upward curve of the calcite solvus. Thus at more typical rain pH values of 4.5, $\Delta Ca^{2+}_{ar} = 0.0158$ mmol/l and $\Delta Ca^{2+}_{ks} = 0.43$ mmol/l, and therefore acid rain neutralization would contribute only 3.5% of the carbonate dissolution.

It should be noted that this example involves the typical situation in which the reaction path originates in the acidic region of the phase diagram and then crosses over into the positive alkalinity region, so that the ΔCa^{2+} has both acid neutralization and karst components. However, in some cases, the reaction path can lie entirely in one region or the other. The calculation of the components are these conditions is summarized in Table 3.

In the case of pure gypsum dissolution, i.e. the rain coming into contact with an accumulated layer of gypsum formed by prior dry deposition reaction with the carbonate stone, the solution chemistry would simply move to the right parallel to the horizontal axis until it reaches the gypsum solvus. There would be no change in alkalinity. If the rain had the pH value of 3.5 then the maximum path length would be 10.5 mmol/l, which is also the value of ΔCa^{2+}_{dd}. Consequently, the dry deposition effect has the potential of contributing 66 times more Ca^{2+} to the solution than acid neutralization.

Therefore the lack of correlation between rainfall pH and runoff Ca^{2+} typically observed in mass balance experiments can be explained by the fact that the maximum acid rain neutralization

Table 3
Calculation of alkalinity components under various pH conditions.

	$pH_{rn} < 5.65$ & $pH_{rf} > 5.65$	$pH_{rn} > 5.65$	$pH_{rf} < 5.65$
ΔCa^{2+}_{ar}	$0.5H^+_{rn} - \frac{10^{-11.6}}{H^+_{rn}}$	0	$0.5\Delta Alk$
ΔCa^{2+}_{ks}	$\frac{10^{-11.6}}{H^+_{rf}} - 0.5H^+_{rf}$	$0.5\Delta Alk$	0

effect is overwhelmed by karst and deposition effects. It should be noted that these calculations were made with the assumption that the solution eventually reaches saturation with respect to either calcite or gypsum. Whether or not this happens in reality depends on the solution's residence time on the stone before it becomes runoff and on the dissolution kinetics of the calcite or gypsum.

Thus far the discussion has assumed that the solution contains only the ions Ca^{2+}, H^+, HCO_3^- and SO_4^{2-}. Other ions may be present in minor concentrations including K^+, Na^+, Mg^{2+}, Cl^- and NO_3^-. However, these do not form solid phases at the concentrations involved, so their effect is mainly to shift the solvus position slightly through their effect on the ionic strength and hence the activity coefficients.

2.2. Bronze attack

A similar approach similar to that can be used to analyze mass balance data for bronze. However, the situation is more complicated because the acid deposition attack would not be primarily on the metal itself, but rather on the corrosion layer, or patina, that forms over time (Kratschmer et al., 2002). For indoor bronze objects the patina is usually composed of copper oxides. However, on outdoor bronze objects, the mature patina consists of two layers with the inner one made up of cuprite, CuO, and the outer layer of brochantite, $Cu_4(OH)_6SO_4$. This hydroxy sulfate mineral, which gives the patina a characteristic bluish-green color, forms by dry deposition even in rural areas (Wu et al., 1992).

Brochantite dissolution in pristine rain is the reaction:

$$Cu_4(OH)_6SO_4 \rightarrow Cu^{2+} + SO_4^{2-} + 3Cu(OH)_2\downarrow \quad (15)$$

This is shown as incongruent dissolution because $Cu(OH)_2$ is stable in the pH range typically found in bronze runoff (Albrecht et al., 2011). It has been difficult to verify this in the field, because the $Cu(OH)_2$ exists as a gel which is difficult to identify in patinas by X-ray diffraction. Moreover, it presumably reacts with environmental sulfate to reform brochantite. Consequently, according to Eqn. (15), the increase in the runoff ions would have a 1:1 M ratio of Cu to SO_4^{2-}. Hence:

$$\Delta Cu_{dd}^{2+} = \Delta SO_{4_{dd}}^{2-} \quad (16)$$

Acid rain is neutralized by brochantite through the reaction:

$$Cu_4(OH)_6SO_4 + 6H^+ + 3SO_4^{2-} \rightarrow 4Cu^{2+} + 4SO_4^{2-} + 3H_2O \quad (17)$$

Since 6 mol of H^+ are consumed for every 4 mol of Cu^{2+} added to the runoff solution, then:

$$\Delta Cu_{ar}^{2+} = -0.667\Delta H^+ \quad (18)$$

Unlike the case of acid rain neutralization by carbonate stone, this reaction also increases the SO_4^{2-} concentration in the runoff in addition to reducing the acidity, but only at the ratio of one mole of SO_4^{2-} for each four moles of Cu^{2+}. Consequently in the case of combined brochantite dissolution and acid rain neutralization, the dry deposition component of Eqn. (16) becomes:

$$\Delta Cu_{dd}^{2+} = \Delta SO_{4T}^{2-} - \Delta SO_{4ar}^{2-} = \Delta SO_{4T}^{2-} + 0.167\Delta H^+ \quad (19)$$

Note that there is no bronze analog to the karst effect component in carbonate stone because there are no copper carbonate minerals present in the patina.

The total ΔCu^{2+} loss is given by the sum of Eqn. (18) and Eqn. (19):

$$\Delta Cu^{2+} = \Delta SO_4^{2-} - 0.5\Delta H \quad (20)$$

which is the correct stoichiometry.

2.2.1. Bronze phase diagram

The various copper minerals that could be found in the patina layer belong to the ternary system $Cu^{2+} - SO_4^{2-} - OH^-$. Hence the solubility diagram is a 3-dimensional surface, which is difficult to visualize. However, as with development of the carbonate stone phase diagram (Section 2.1.4 above), since the incident rainwater is nearly pure water, the chemistry of the solution in contact with the patina is dominated by its mineral assemblage. Hence the electroneutrality condition can be approximated by:

$$2Cu^{2+} + H^+ = OH^- + 2SO_4^{2-} \quad (21)$$

This can then be used to substitute for Cu^{2+} in the solubility products to yield the 2-dimensional diagram of the patina stability shown in Fig. 2 with axes of pH and SO_4^{2-} (Livingston, 1991). In contrast to the carbonate phase diagram (Fig. 1), logarithmic scales are required because the concentrations range over several orders of magnitude. Also, activities have been used because of the higher ionic strengths involved. The stable phase under typical rain acidity conditions ($3.5 < pH < 6$) would be brochantite, which is consistent with field observations. The diagram also predicts that under high sulfate concentrations, antlerite becomes the stable phase instead. However, this phase has rarely been observed in the field, usually only under sheltered exposure conditions (Kratschmer et al., 2002).

Finally, the diagram also predicts that the stable phase under high pH and low sulfate conditions would be tenorite (CuO). However, this has not actually been observed in the field. Its presence in the phase diagram is a formal result, due to the uncertainties in the thermodynamic data on the more likely phase, $Cu(OH)_2$. This can occur as a gel, and its free energy of formation depends upon the surface area of its colloidal particles, which can vary significantly (Stumm and Morgan, 1981).

As discussed in Section 2.1.4 above, the lowest pH that has been observed in rainfall is roughly 3.5. This is marked as point **a** in Fig. 2. The reaction path resulting from the neutralization of acid rain is shown by the line segment ab. This intercepts the brochantite solvus at point **b**, which has the coordinates: pH = 5.56,

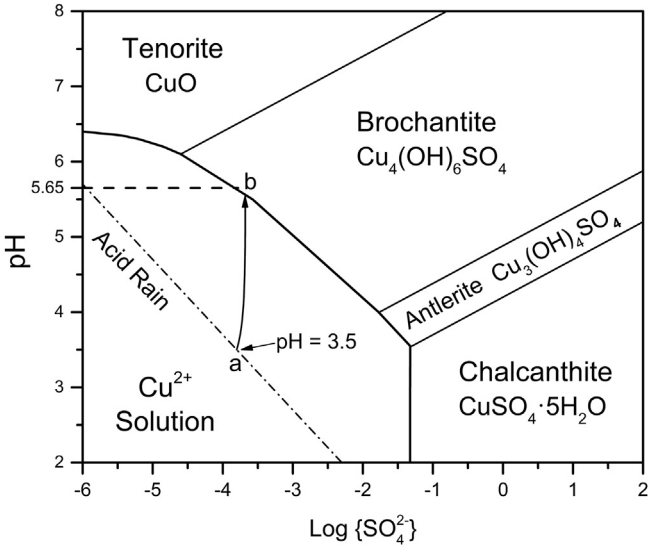

Fig. 2. Bronze patina/acid rain phase diagram.

$SO_4^{2-} = 0.21$ mmol/l, which corresponds to a ΔCu_{ar}^{2+} of 0.21 mmol/l. The reaction path of simple dissolution of brochantite in a solution initially at point **a** would be parallel to the horizontal and eventually would intercept the solvus of chalcantite at $SO_4^{2-} = 47.3$ mmol/l which implies $\Delta Cu_{dd}^{2+} = 47.3$ mmol/l. Thus the maximum amount of copper that could be lost per rain event by brochantite dissolution, and hence dry deposition, is 225 times that lost by acid rain neutralization.

3. Statue of *Phoenicia* carbonate stone mass balance case study

In a recent review of the literature on air pollution and stone deterioration, Steiger (2015) listed 13 studies that concerned measurements in the field. The vast majority used either mass loss or surface recession to characterize stone damage. Neither of the two investigations that did use mass balance – O' Brien et al. (1995) and Cardell-Fernandez et al. (2002) – utilized geochemical modeling of the runoff. To illustrate the value of this modeling approach, it is applied here to a data set from a field study in New York City. Although this data set was collected in the early 1980s, it is the only one available, and it remains valid for demonstrating the use of geochemical models to analyze the results mass balance method on carbonate stone.

This method was applied to a Holston marble statue, located on the cornice of the Alexander Hamilton Custom House, Fig. 3, which is sited on the southern tip of Manhattan Island in New York City (Livingston et al., 1982).

The statue *Phoenicia* was chosen over the 11 other statues at the site because of her relatively simple geometry which facilitates the collection of runoff. She is nine ft. (274 cm) tall and stands on a 40 in.(101 cm) by 40 in. (101 cm) base, which is located on the sixth-floor cornice level of the North facade as shown in Fig. 3. This location, 100 ft. (30.5 m) above the ground, eliminates the complications from groundwater, road salt and other causes of stone deterioration found at street level. The statue is mounted in such a way that it is exposed on all sides to the atmosphere and to rainfall.

Phoenicia was put in place in 1906 and thus had 75 years of exposure to the weather and air pollution at the time the runoff measurements were made. During this period sulfur dioxide levels in the Manhattan area are estimated to have peaked in the 1950s, but no monitoring data are available for that period. The earliest records, from 1967, show levels as high as 420 μgm/m^3 (Ferrand and Blade, 1969). As discussed in Section 5, subsequent air pollution control measures reduced the level significantly to the point where the concentration of SO_2 averaged 47 μgm/m^3 at the time of the mass balance measurements (Delaware, 1982). Visual inspection showed a characteristic pattern of light-colored stone in the areas washed by rain, and darker areas including some biological growth in the rest of the surface.

3.1. Data collection

The procedure called for collecting simultaneous samples of water of incident rain and of the resulting runoff from the statue. The samples were then analyzed using the U.S Environmental Protection Agency's standard protocol precipitation quality analysis for concentrations of several specified ions, i.e. sulfate, nitrate, ammonia, chlorine, calcium, magnesium, potassium, sodium and phosphate (Rockwell International, 1982). Also measured in both kinds of samples were pH and conductivity. The runoff collection apparatus consisted of plastic guttering fixed around the perimeter of the base of the statue.

The incident rainfall was collected in 5 gallon glass containers fitted with large plastic funnels. These containers remained permanently on the roof as passive samplers, collecting all the rainfall that fell over the duration of the sampling cycle. This approach, in which the collector is always open, also collects particulate matter during dry periods, and is known as bulk collection, as opposed to collectors that collect only during precipitation. However, this approach more accurately represents the situation on the statue's surface, which would also collect particulate matter during dry intervals. The analyses were performed by Environmental Protection Agency staff at the Edison Laboratory in Edison, N.J. Atomic absorption spectroscopy was used for the metals and ion chromatography for the anions. The precision of these analyses is typically 1–2%.

A total of 23 runoff samples were collected. However, due to lack of sufficient volume of rainfall samples for the earlier events, only the 8 most recent cases could be fully analyzed. These were taken in the months of March through May of 1981.

Before calculating the mass balances, the solution chemistry has to be adjusted for carbonate species and ion pairing. Calcium and sulfate ions form a neutral species $CaSO_4$ by ion pairing, which accounts for 30% of the total gypsum solubility. However, the atomic absorption analytical method gives total calcium i.e. the

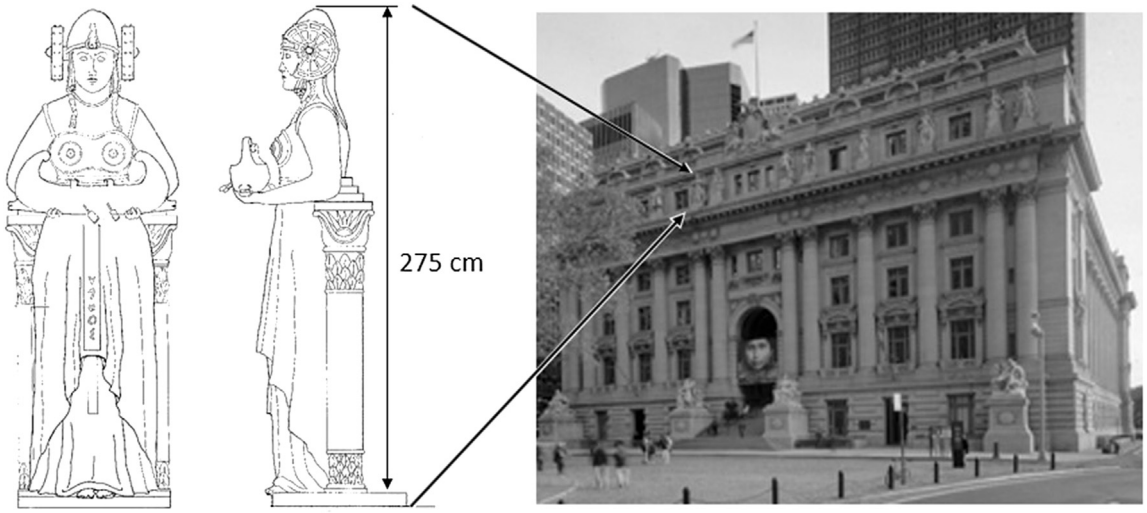

Fig. 3. The Statue of Phoenicia and the Alexander Hamilton Custom House site.

sum of Ca^{2+} and the calcium in $CaSO_4$.

On the other hand, ion chromatography gives only SO_4^{2-} ion, not total sulfate. After these adjustments to the individual solutions, the runoff-rainfall differences can be calculated.

The increase in Ca^{2+} ion in the runoff is plotted against the pH of the rain in Fig. 4. It can be seen that there is no correlation. Also plotted in this figure is a horizontal line at 0.158 mmol/l representing the maximum increase that could be achieved by acid rain neutralization assuming a historically low pH of 3.5 as discussed in Section 2.1.4. All of the data points plot above this line, indicating that the karst and dry deposition components dominate over acid rain neutralization.

3.2. Reaction path plots

The *Phoenicia* data rain-runoff reaction paths are plotted in the phase diagram for carbonate/acid rain (see Fig. 1) as vectors in Fig. 5a. However, the paths are so small that for better visibility the region containing them is plotted in an enlarged version in Fig. 5b. They are all strongly slanted toward the horizontal, which indicates that gypsum dissolution and hence dry deposition dominates. Except for two cases, they all cross over into the karst effect region indicating a significant ΔCa_{ks}^{2+} component. The remaining two cases actually originate in this region, which means that the rain was alkaline, rather than acidic, to begin with.

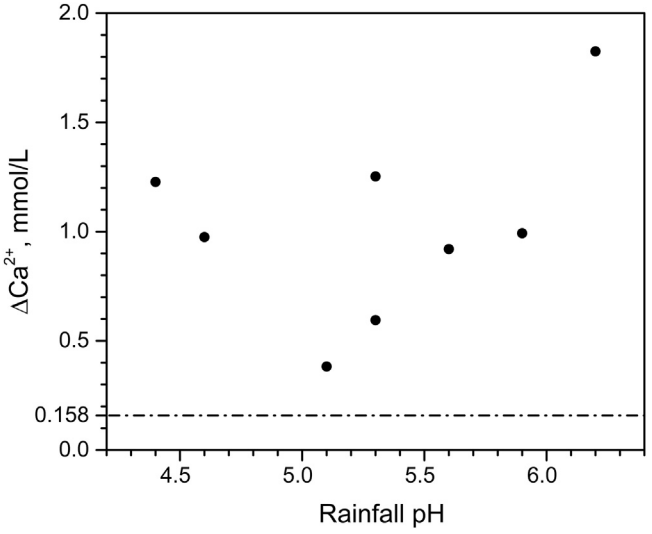

Fig. 4. Plot of calcium ion increase in runoff versus rainfall acidity. The horizontal dash-dot line at 0.158 mmol/l is the maximum ΔCa^{2+} achievable through acid rain neutralization.

It can be seen in Fig. 5a that none of the paths reach equilibrium with calcite. This violates a key assumption of the Lipfert Equation, which has been used to predict carbonate stone damage (Steiger, 2015). In this case, the residence time of the solution on the surface appears to have been too short to reach saturation with respect to calcite.

Concerning the sulfate component, there is the question of the possible presence of gypsum on or in the surface remaining from higher historic pollution levels. However, taking destructive samples from the surfaces of sculptures is usually prohibited. Therefore, it is not possible to answer this question directly in the case of the Statue of *Phoenicia*. Moreover, even if sampling were permitted, it cannot be assumed that any gypsum found would be due solely to "historic" pollution. In the absence of any such deposits, gypsum would still accumulate between rain events because of dry deposition from current ambient levels of SO_2 and sulfate particulate matter. Whether or not this accumulation is quantitatively removed in the succeeding rain event depends upon a number of random variables including dry deposition rate, time interval between rain events, the volume of the rain event and runoff flow parameters. Thus at any point in time there could be a layer of gypsum on the surface that may be due to dry deposition over the preceding days or months, but not from historic, meaning previous years to decades, pollution.

Moreover, based on visual inspection of the Statue, it is unlikely that there would be much historic gypsum on the areas actually washed by rainfall. These areas appear to be relatively white and clear of any crust, while thick layers of characteristically black gypsum crust are seen on other parts of the Statue that are sheltered from rainwater. This is a general pattern seen on carbonate stone structures exposed to sulfate dry deposition. In those cases in

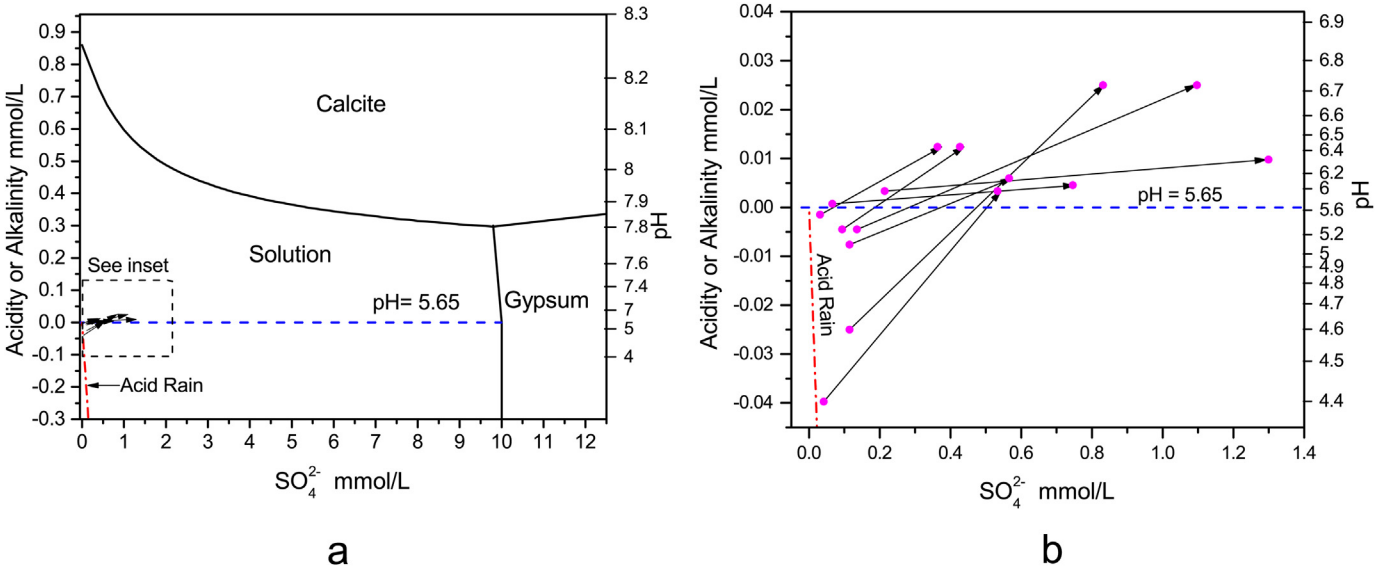

Fig. 5. a. Reaction paths of *Phoenicia* data plotted as vectors in the carbonate/acid rain phase diagram. **b** Enlarged view of the region in Fig. 5a containing the reaction paths of *Phoenicia* data.

which surface samples could be taken of the washed areas, negligible gypsum was found (Camuffo et al., 1982; Davidson et al., 2000). Since the same spatial pattern has been seen in historic photographs even in periods when the ambient SO_2 concentrations were significantly higher (Davidson et al., 2000), this implies that rainwater is an effective agent of dissolution that prevents the accumulation of significant layers in the washed areas.

3.3. Acidic deposition components

A minor increase in NO_3^- ion was observed in every event. To highlight this, the three component model of Eqn. (10) was rewritten to include a nitrate dry deposition term:

$$\Delta Ca_T = \Delta SO_{4_T} + 0.5\Delta NO_3^- + 0.5\Delta Alk \quad (22)$$

where the subscript T indicates the sum of Ca^{2+} or SO_4^{2-} together with its counterpart in neutral $CaSO_4$.

The components are plotted in a bar graph in Fig. 6. It can be seen that ΔSO_4^{2-} is much larger than the contribution of the other anions in every sample. The next largest component is ΔNO_3^- Thus the combined dry deposition processes dominate over the acid neutralization and karst processes as the major mechanism of marble mass loss in this situation.

A striking feature of Fig. 6 is that except for Event #7, there is always a significant excess of ΔCa_T. This indicates that there some other process beyond the ones involved in karst and acid deposition that is attacking the calcite. For Event #7 on the other hand, the Ca^{2+} deficit means that there is some unmeasured cation present. This violates the assumptions of the three component model and therefore this data point is excluded from further analysis.

3.4. Calcium and chloride ion imbalances

To investigate the causes of the imbalances shown in Fig. 6, it is necessary to consider the other ions present in the runoff. The full electroneutrality condition including all the measured ions is:

$$2Ca^{2+} + 2Mg^{+} + K^{+} + Na^{+} + NH_4^{+} + H^{+} = 2SO_4^{2-} + NO_3^- + Cl^- + HCO_3^- \quad (23)$$

The only other anion in this set that could serve as a counter ion for the excess Ca^{2+} is Cl^-. Inspection of the data shows that both Na^+ and Cl^- are present in significant concentrations, which presumably is the result of sea salt deposition. From the stoichiometry of pure sodium chloride, these two ions should have a 1:1 ratio, but in sea-salt the actual Cl:Na ratio is 1.174 due to the presence of other ions in seawater (Zhuang et al., 1999). Applying this ratio to the data yields a significant excess of Cl^- over Na^+, which is thus available to balance the Ca^{2+}. The Ca^{2+} imbalances are compared against this difference, denoted as (Cl-Na), in Fig. 7, and they all show that excess Cl^- can account for at least part of the observed Ca^{2+} imbalance.

The simple exchange reaction between sea salt and calcium carbonate:

$$CaCO_3 + 2NaCl \rightarrow Na_2CO_3 + CaCl_2 \quad (24)$$

is ruled out based on thermodynamic considerations. Sodium chloride and calcium carbonate form a stable equilibrium mineral assemblage under ambient conditions.

A possible source for the excess Cl component is the sea salt dechlorinization (SSD) reaction in coastal areas between sea salt particles and nitric acid vapor to produce hydrochloric acid vapor:

$$HNO_3 + NaCl \rightarrow NaNO_3 + HCl\uparrow \quad (25)$$

The nitric acid vapor is a product of a complicated chain of reactions in the atmosphere beginning with nitrogen oxides (NO_x) emitted from combustion processes (Moussiopoulos et al., 1995). Evidence for SSD is found in the bulk chemistry of the coarse fraction of particulate air pollutants, which shows a depleted chloride content relative to sodium (Bardouki et al., 2003). Complementary evidence is the increase in Cl in rainwater samples due to HCl absorption (Shapiro, 2007). In addition, TEM examination of individual coarse particles have shown complete Cl depletion (Roth and Okada, 1998). A review of the literature on SSD is given by Evans (2003).

Data relevant to SSD in the New York City area are very scarce. A major campaign of particulates matter monitoring was carried out at the Queens College site in Manhattan in the early 2000's (Drewnick et al., 2004). However, the analysis did not include Na or Cl. The coarse particulate fraction (>2.5 μm) did show nitrate concentrations that are indicative of SSD.

Even after taking into account the SSD effect, Fig. 7 shows that there still remains a significant positive Ca^{2+} imbalance in the runoff, associated with some unknown counter ions. The most likely candidates are organic acids, which were not included in the

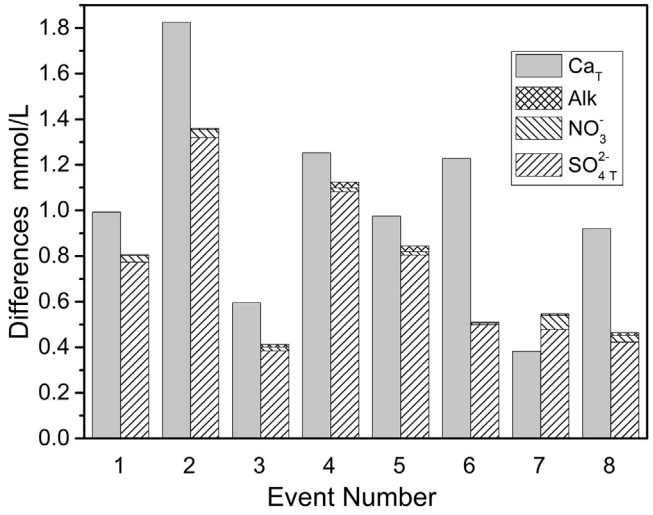

Fig. 6. Comparison of Ca_T vs acid deposition components.

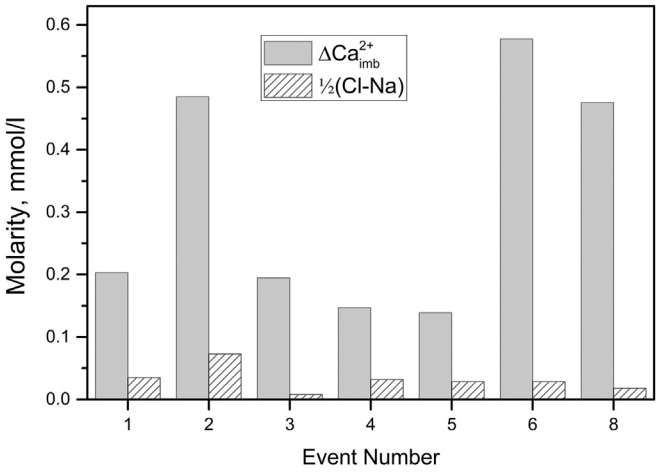

Fig. 7. Comparison of Ca imbalance vs excess Cl.

protocol for solution analysis. When the organic content of rain water has been explicitly analyzed, it has been dominated by low-molecular weight carboxylic acids such acetic, oxalic, formic, pyruvic etc (Souza et al., 1999). These organic acid aerosols and vapors are biogenic, but they can be produced by a number of anthropogenic sources such as chemical plants, incinerators and automobiles (Chebbi and Carlier, 1996).

3.5. The five component model

With the assumption that remaining Ca^{2+} imbalance can be assigned to unmeasured organic acids, it is possible to write the overall charge balance in terms of five components:

$$\Delta Ca^{2+} = \Delta SO_4^{2-} + 0.5\Delta NO_3^- + 0.5\Delta(Cl^- - Na^+) + 0.5\Delta Alk + \Delta Organics \quad (26)$$

The relative importance of each of these components can then be expressed as a percentage of the total amount of dissolved calcium. The mean values of these percentages are plotted in Fig. 8.

As noted previously, the sulfate dry deposition process dominated the marble attack under the environmental conditions prevailing in the New York City region in the early 1980s, accounting for over 69% of the dissolved calcium. Next in importance was the inferred organic component, at roughly 26%. As shown in the inset of Fig. 8, the chloride component was third at just under 3%. The nitrate dry deposition and the total alkalinity components were comparable, around 1%.

For the latter, the karst effect contributed 0.8% and the acid rain neutralization about 0.3% of the total loss. Thus the magnitude of the acid rain component was much less than the uncertainties in the dry deposition component.

As discussed in the Introduction, mass-balance studies do not measure surface recession. However, it is possible to calculate an estimated surface recession from the ionic concentrations by making some assumptions about the weathering process and the annual rainfall volume. As an example, the mean ΔCa^{2+} in the seven runoff events measured on the statue of *Phoenicia* was 1.1 ± 0.4 mmol/l or 44.6 ± 14 mg/l, given the Ca atomic weight of 40.08. Characterization of Holston marble reveals that is essentially pure calcite with a very low porosity, 0.31 ± 0.09% (Aloiz et al., 2012). Therefore, its density can be approximated by that of crystalline calcite, 2.71 g/cm^3. Hence the volume of stone removed per liter of runoff is 44.6/2.71 = 0.0164 cm^3/l.

The average annual rainfall in the Eastern United States is roughly 100 cm per cm^2 or 0.1 liter (NOAA, 2015). This yields an estimated surface recession of 16.4 μm/yr. For comparison, actual surface recession rates measured with a microerosion meter on limestones in temperate climates are in the range of 10–40 μm/yr (Stephenson and Finlayson, 2009). The estimated surface recession rates for the various components of the carbonate attack on *Phoenicia* can be read off on the right hand vertical axis in Fig. 8.

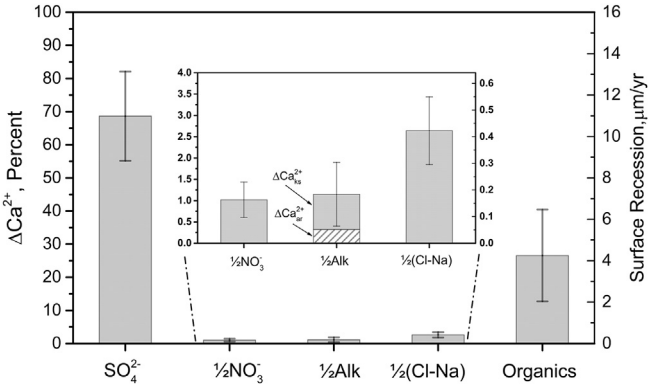

Fig. 8. Mean values of carbonate attack components (7 events), expressed as percentage of total dissolved calcium on the left vertical axis. Estimated surface recession is given on the right vertical axis.

Finally, since the method of rainfall collection used a sampler that was always open, there is the possibility that some dry deposition occurred on the collection funnel between rain events. To understand the possible effects of this on the estimated dry deposition component, it is necessary to consider dry deposition by acidic gases separately from deposition by particulate matter. Only the latter occurs in the open collector because the polyethylene funnel is nonreactive to the acidic gases. In contrast, the dry deposition rate on the carbonate stone of the Statue is the sum of both processes. Moreover, the major acidic anion, sulfate, in the particulate matter can be in either a reactive species such as NH_4HSO_4 or as particles of inert calcium sulfate, gypsum. Presumably the latter type of particle simply lies on the surface until washed off by rainfall. With the open collector method, the measured concentrations are thus the sum of the both the constituents in the incident rainfall and any dissolved dry deposition particulate matter. The effect of the reactive particles would be to reduce the pH of the collected solution while increasing the sulfate concentration over the values in the incident rain. The effect of the inert particles would be to increase both the calcium and sulfate concentrations over the incident rain levels without changing the pH.

The dry deposition component of the 3 component model is calculated as the difference in the sulfate concentration between the rainfall and the runoff. If the dry deposition in the open rainfall collector consisted only of inert gypsum, this subtraction would simply be a correction for any inert sulfate particle deposition on the Statue surface. In this situation there are no acidic particles and hence the difference would be the dry deposition rate by SO_2 on the Statue. In the case of acidic particles in the dry deposition, their sulfate concentration in the solution from the rainfall collector would also be subtracted from the runoff solution. This would have the effect of underestimating the total dry deposition rate on the Statue.

Although there was no direct measurement of the dry deposition rate on the rainfall collector, it is possible to make an estimate of this effect by examining in detail the composition of the solutions from the runoff collector. The ratio of SO_4^{2-} in the rainfall solution to SO_4^{2-} in the runoff ranged from 0.08 to 0.21. However, some fraction of the rainfall sulfate could be in the form of inert gypsum. This fraction in turn can be estimated by considering the calcium to sulfate ratio in the rainfall solution. This ranged from 0.59 to 1.52. The Ca^{2+}concentration can regarded as a proxy for gypsum dry deposition since the Ca^{2+}concentration of rain as measured by the National Trends Network has remained at a fairly constant level of 0.1–0.2 mg/l from 1985 to 2014 (NADP, 2014), whereas in solutions from the open rainfall collector at the statue of *Phoenicia* it was orders of magnitude larger, in the range of 1.2–13.0 mg/l. Adjusting the sulfate ratio for this inert fraction yields a maximum underestimate of the acidic particle dry deposition rate of 12.6%. This is comparable to the uncertainty of 13.5% in the mean value of the dry deposition component (Fig. 8). Moreover, the fact that this is an underestimate implies that the actual dry deposition component would be larger, thereby strengthening the conclusion that this component dominates the attack on carbonate stone.

4. Gettysburg bronze plaque case study

Tidblad (2015) has recently reviewed the literature on air

pollution damage to metals. However, most of the studies of bronze were based on weight loss measurements. Moreover, they typically used freshly prepared bronze specimens, but it takes a decade for the two layer cuprite and brochantite patina to develop. There are very few data sets of runoff collected from bronze with mature patinas. Zhang et al. (2002) did conduct such a study, but measured only the cations in the runoff. The absence of data on anions thus ruled out the application of geochemical modeling. To illustrate this modeling approach for bronze, it is applied here to a data set collected from bronze memorial plaques at the Gettysburg National Military Park in Gettysburg, Pennsylvania (Meakin et al., 1992). Although these data sets were collected in the early 1980s they are the only ones available, and they remain valid for demonstrating use of geochemical models to analyze the results of the mass balance method. These measurements were made on three bronze memorial plaques (see Fig. 9) which were cast with a 95% Cu/5% Zn bronze and put in place in 1906.

4.1. Data collection

Runoff samples were collected for 38 individual rain events at each of the three sites during the period 1986–88. The rain and runoff samples were analyzed for the ions Cu^{2+}, Zn^{2+}, Mg^{2+}, Ca^{2+}, SO_4^{2-} and NO_3^-. The solution variables pH and conductivity were also measured. However the data for several samples had to be discarded because of incomplete chemistry analysis.

The Cu^{2+} concentration in the runoff is plotted against the pH of the incident rain in Fig. 10, but there is no apparent correlation. Also plotted in Fig. 10 is the horizontal line at $Cu^{2+} = 0.21$ mmol/l, which is the maximum value that could be achieved by neutralization of acid rain, as discussed in Section 2.2.1. It can be seen that the actual concentrations significantly exceed this limit in most cases. This indicates that the process of brochantite dissolution dominates over the effect of acid rain neutralization.

Fig. 9. The bronze memorial plaque for the 2nd Brigade, 2nd Division, III Corps of the Union Army at Gettysburg National Military Park; one of three such plaques used in the mass balance study.

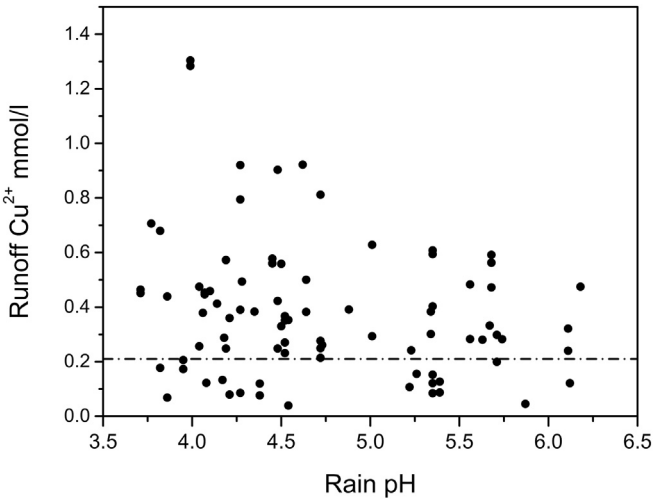

Fig. 10. Plot of Cu^{2+} in runoff versus rain pH. The dash-dot line at $Cu^{2+} = 0.21$ mmol/l indicates the limit for acid rain neutralization.

4.2. Reaction path analysis

Before applying the two component model developed in Section 2.2.1 above, it was necessary to filter the data to remove cases which showed a significant mass imbalance, thus indicating the presence of unanalyzed ions. The screening criterion was based on the ratio of the total cation to the total anion charge. If this ratio for a specific event was less than 0.9 or greater than 1.1, its data was discarded. Out of a total of a potential total number of 83 only 15 passed the screening process. Some possible causes of the imbalances are discussed in Section 4.4 below.

The screened data are plotted as a vector for each event, starting at the rain composition and ending at the runoff composition, in the patina/acid rain phase diagram in Fig. 11. None of the vectors reach the solvus line. They are all undersaturated with respect to brochantite, either because the contact time with the patina was not long enough or because the runoff mixed with some incident

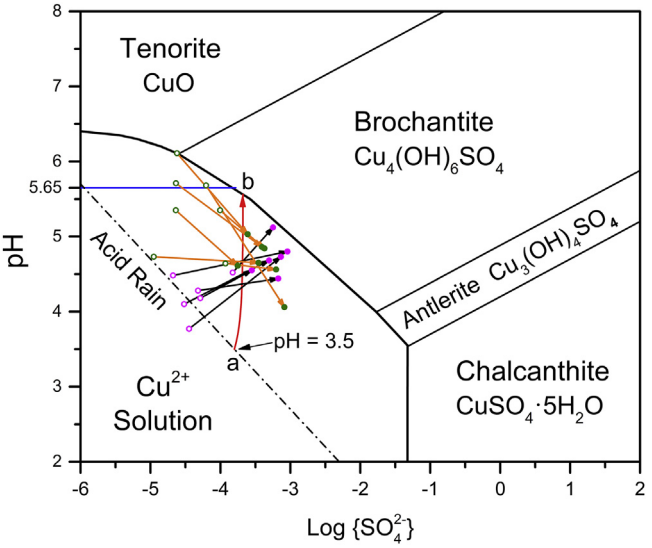

Fig. 11. Rain-runoff vectors plotted in the patina/acid rain phase diagram.

rain while running over the surface.

The vectors all slant toward the right, indicating a significant dry deposition component. However, seven vectors, marked in orange, slope downward rather than upward, which means that the acidity actually increased in the runoff compared to the rain. Since neither brochantite dissolution nor acid rain neutralization can produce this effect, some other reaction with the surface must be occurring. As discussed in Section 4.4 below, the most likely possibility is oxidation of cuprite to copper hydroxide. This does not result in additional copper loss in the runoff, but it does confound the use of the two component model to estimate acid rain neutralization. Therefore, these seven cases were removed from further analysis.

Finally, several vectors have starting points that plot to the left of the dashed line which represents the composition of a pure dilute sulfuric acid solution. This indicates the presence of some NO_3^- ion in the rain. This does not affect the application of the two component model which uses only the total acidity of the rain, not the individual acidic species.

In order to see the vectors more clearly, an enlarged version of the area in Fig. 11 that contains them is plotted in Fig. 12 using linear axes of SO_4^{2-} and alkalinity. Note that the two axes have different scales. Also, as described in Section 2.2.1, the acid rain neutralization component contains a small amount of ΔSO_4^{2-}, thus it is not orthogonal to the dry deposition component.

Fig. 12 includes a diagram in the lower right hand corner showing the relative sizes and orientations of the two components for a unit increase in each. It can be seen that all the vectors slant strongly toward the horizontal axis, indicating dominance by brochantite dissolution.

To verify that the electroneutrality condition of Eqn. (21) correctly characterizes these cases, a linear regression analysis of the observed ΔCu^{2+} versus the difference ($\Delta SO_4^{2-} - 0.5\Delta H$) was made. This gave a moderately good fit, $R^2 = 0.91$, but the slope was 1.28 instead of the correct 1.0. Including a nitrate dry deposition component led to the model:

$$\Delta Cu^{2+} = \Delta SO_4^{2-} + 0.5\Delta NO_3^- - 0.5\Delta H^+ \quad (27)$$

As shown in Fig. 13, this gave a very good fit to the data, $R^2 = 0.99$, with a slope of 0.93. Including Zn^{2+} into the regression did not produce a significant improvement in the fit. The Zn^+ ratio to Cu^{2+} in the runoff was a relatively constant 2.5% ± 0.4% which implies collinearity.

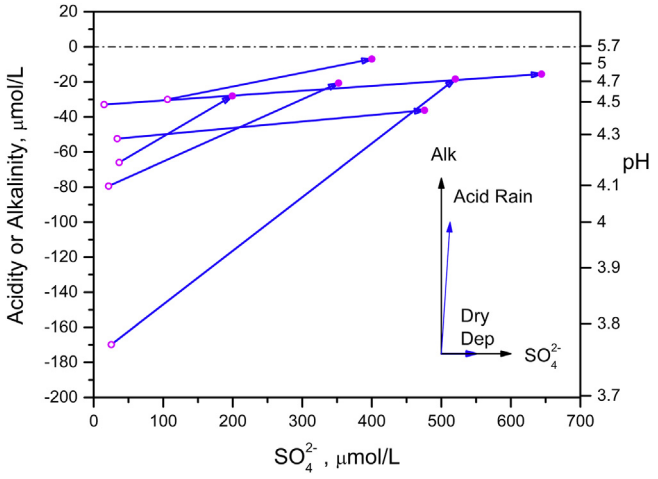

Fig. 12. Enlargement of the region in Fig. 11 containing reaction path vectors. Inset diagram shows the relative size and orientation of the two components for this set of axes.

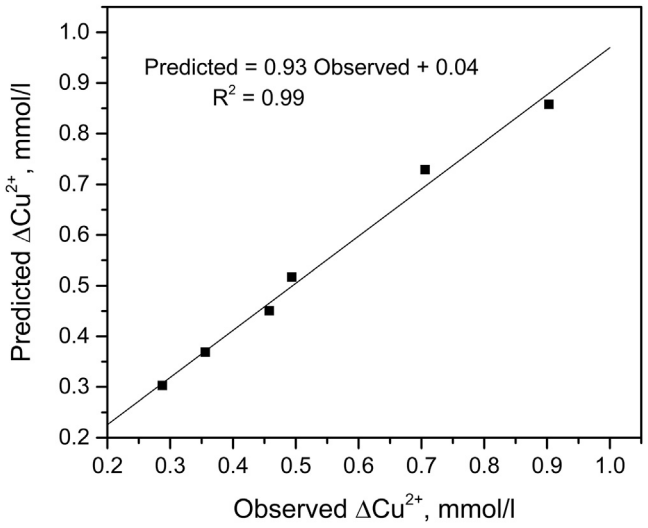

Fig. 13. Plot of observed copper loss versus predicted loss using the three component model of Eqn (27).

Using the model of Eqn (27), it is possible to partition the observed total copper loss into three components: acid neutralization, brochantite dissolution and dissolution of a copper nitrate phase formed by NO_3^- dry deposition, which may be a copper ammonium nitrate compound as discussed below in Section 4.4 below. The relative magnitude of each of these three components is plotted for each event in the bar graph in Fig. 14. These results are summarized in the plot of mean values in Fig. 15 which shows that the largest component is SO_4^{2-} dry deposition with a mean value of 70.6%. Second is NO_3^- dry deposition at 23% and finally, the mean value for acid rain neutralization is 6.4%.

An estimated surface recession rate can be calculated for the bronze plaques using same approach as described above for the Holston marble. The mean ΔCu^{2+} in the runoff is 0.54 ± 0.2 mmol/l or 34 mg/l. The density of copper metal is 8.94 g/cm^3. Hence the volume of copper loss in the runoff is 3.82 mm^3/l. For an annual rainfall volume of 100 cm/cm^3, this gives a surface recession rate of 3.82 µm/year. The only available information on surface recession rates of copper statues is for the Statue of Liberty. Baboian and

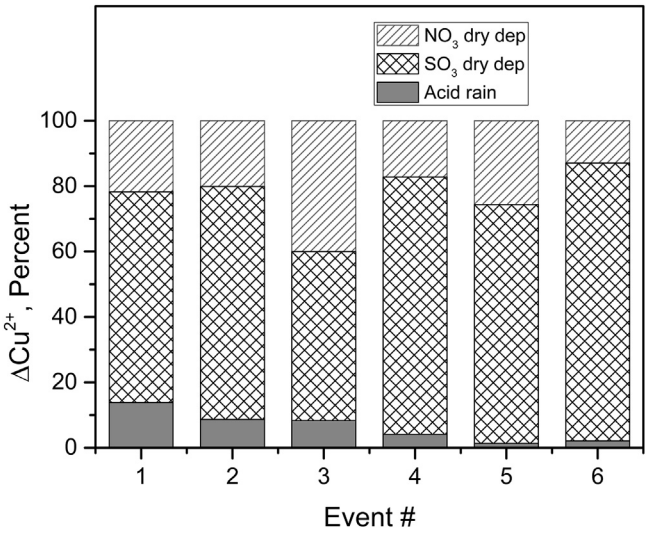

Fig. 14. Plot of relative magnitude of the bronze attack components in individual events.

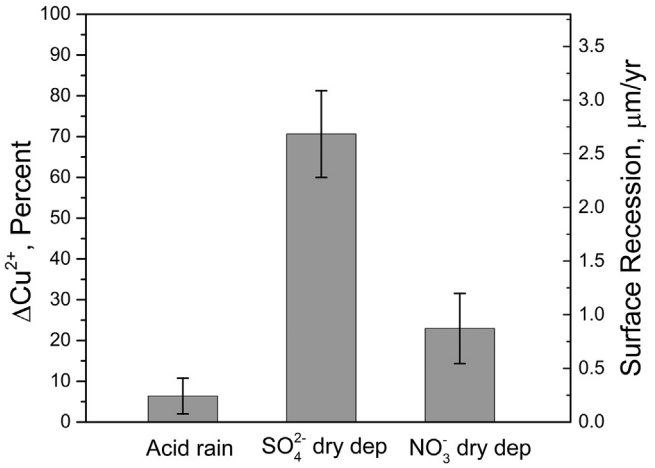

Fig. 15. Mean values of bronze attack components. Percentages are plotted on the left vertical axis and estimated surface recession on the right vertical axis.

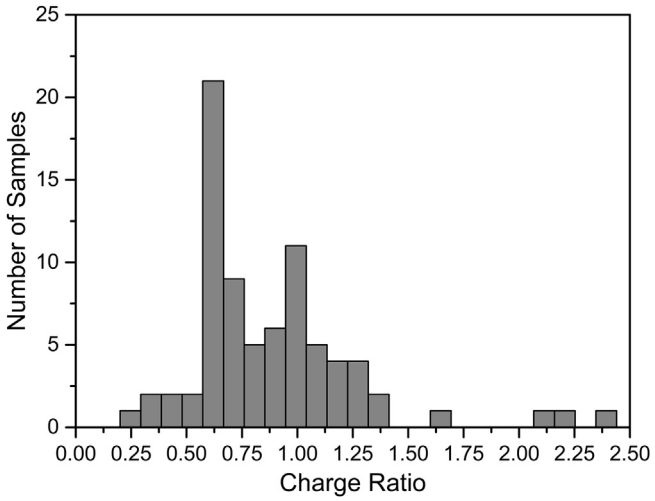

Fig. 16. Histogram of charge ratios for all events.

Cliver (1986) measured a thickness loss of the Statue's copper skin of 1.3 ± 0.2 μm/yr averaged over 100 years. This compares well with the estimated surface recession of the bronze plaques given the uncertainties in the assumptions that are required. The surface recessions of the individual components of bronze attack can be read off Fig. 15 using the right hand vertical scale.

4.3. Minor ions

Concerning the other measured ions that are not involved in the model of brochantite removal, runoff–rainfall differences in Ca^{2+} and Mg^{2+} are at least an order of magnitude lower than the major ions and do not show any consistent patterns. In some cases, the latter is actually negative.

Finally, the Cl^{-} differences are larger, but more variable. Since Gettysburg is located roughly 90 km inland from the nearest seawater, sea salt particle deposition is unlikely. A more likely possibility would be road de-icing salts since the memorial plaques are sited close to the major north-south road through the battlefield. Both NaCl and $CaCl_2$ are used for de-icing salts. However, the Ca^{2+} and Cl^{-} differences are not correlated, and Na^{-} was not among the analytes.

4.4. Charge imbalances

Although the data for a large number of samples could not be used for the two component model because the charge ratio fell outside the range of 1.0 ± 0.1, it is still possible to extract some information from these data. A histogram of the charge ratio is plotted for all samples in Fig. 16. Roughly 64% of the samples had a charge less than 0.9, indicating the presence of unanalyzed cations. The most likely candidate is NH_4^+ from dry deposition of ammonium sulfate and nitrate fine particulate matter. However, ammonium ion was not included as an analyte in Gettysburg study.

Lobnig et al. (1994) and Lobnig and Jankoski (1998) have demonstrated that ammonium sulfate particles can react with copper with the end result being brochantite, but this reaction only occurs above a critical relative humidity of 80% at 300 K. Consequently it is possible that under certain environmental conditions, some unreacted ammonium sulfate particles were present on the surface and dissolved in the runoff. Also, Bassett and Durrant (1922) found that ammonium nitrate reacts readily with copper to form basic copper nitrate, $Cu_4(OH)_6(NO_3)_2$. This could account for the significant amount of NO_3^- in the runoff. Ammonium compounds including ammonium sulfate are constituents of a number of formulae used in the artificial patination of bronze objects (Hughes and Rowes, 1991). Their function is to accelerate the formation of the patina. This suggests that the deposition velocities of sulfate and nitrate on bronze could be enhanced as ammonium particulate matter compared to those of the gas phases SO_2 or NO_x. Unfortunately, no data are available for data for either ammonia gas or ammonium particulate matter phases available for the Gettysburg area during the 1986–1988 time frame.

Finally for the remaining 26% of the data the cation/anion charge ratio is greater than 1.1. This indicates the presence of unanalyzed anions, possibly the carboxylic organic acids discussed in Section 3.4.

4.5. Acidity increases

In the full data set, roughly 38% of the samples showed an increase in H^+ in the runoff over the incident rain. Since this is not possible for any of the reactions discussed in Section 2.2, this implies that some other process must be taking place. The most likely is oxidation of cuprite to $Cu(OH)_2$:

$$Cu_2O + H_2O \rightarrow Cu(OH)_2 + 2H^+ \quad (28)$$

This suggests that under some conditions, the rain is coming into direct contact with the cuprite inner patina layer. This would be possible if the area coverage of the outer layer of brochantite was not complete, or if this layer was so thin that it could be totally dissolved during a rain event. The implication is that the two layer structure of the patina is not static. Instead, it is dynamic, the result of the competing processes of brochantite formation by dry deposition and dissolution in runoff.

5. Trends in acid deposition attack

The results of the two case studies indicate that acid rain attack played a very minor role in the weathering of marble and bronze outdoor sculpture compared to dry deposition in the 1980's. Moreover, rain acidity has been dropping since then (NADP, 2014). However, SO_2 levels have also been dropping for decades in urban areas in N. America as illustrated in Fig. 17 by the specific case of New York City (Delaware, 1982; Ferrand and Blade, 1969; NYDEC, 2012). This implies that dry deposition may be less significant at present compared to “background” processes of the karst process

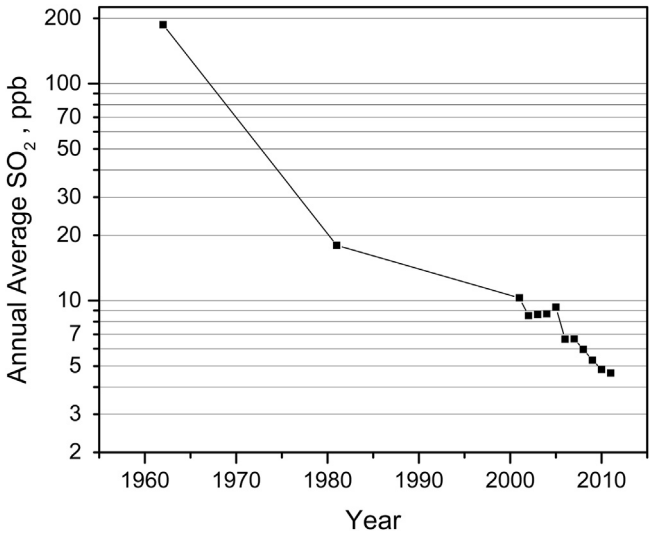

Fig. 17. Trend in annual ambient SO_2 concentrations in New York City, 1964–2010.

and organic acid attack. Consequently, the weathering rates of outdoor sculpture would be regressing back to pre-industrial levels, at least in N. America and Western Europe. However, not enough monitoring data is available for other parts of the globe to make any assessments of deposition levels in those regions (Vet et al., 2014).

The potential effects of organic acids is an area of great uncertainty. Indirect evidence suggests that these could play a role in both carbonate stone and bronze weathering. However, information concerning their ambient concentrations and deposition rates is very sparse (Chebbi and Carlier, 1996). It includes both biogenic and anthropogenic components. Vet et al. (2014) conclude that although the former dominates the emissions, the latter is increasing.

6. Conclusions

In order to understand the counterintuitive lack of a correlation between rain pH and loss by chemical dissolution of sculptural materials, an aqueous geochemical modeling approach was used to analyze rain runoff chemistry for the relative importance of acid rain neutralization, dry deposition, and in the case of marble, natural carbonate dissolution. This approach involved the development of pH – SO_4^{2-} phase diagrams for marble (calcium carbonate) and bronze (copper) under ambient environ-mental conditions. This then enabled reaction path modeling of the acid neutralization process using the pH range typically found in wet deposition (3.5–6). The results were for marble that the theoretical maximum amount of Ca^{2+} ion that could be lost due to acid rain neutralization would be 0.158 mmol/l compared to 10.5 mmol/l by dry deposition, and for bronze, the Cu^{2+} ion losses would be 0.21 mmol/l and 47.3 mmol/l respectively. Consequently dry deposition effects on these materials have the potential to dominate over wet deposition effects.

To test these predictions the geochemical models were applied to examples of data sets from mass balance (runoff vs rainfall) studies on a marble statue in New York City and some bronze memorial plaques at Gettysburg PA. For the marble statue, the mean Ca^{2+} losses by dry deposition was about 69% of the total compared to 0.3% for acid rain neutralization, which was less than the natural carbonate dissolution losses of 0.8%. For the bronze, the mean Cu^{2+} losses were 70.6% by SO_4^{2-} dry deposition and 23% by NO_3^- dry deposition compared to 6.4% by acid rain neutralization. Thus for both cases the wet deposition component was less than the variability of the dry deposition components which explains the observed lack of correlation between the rain pH and the material losses. In addition, for the marble case, there was evidence for HCl acid vapor attack resulting from nitric acid/sea salt interactions and for bronze, ammonium ion may be important. For both cases, significant imbalances suggested that unmeasured organic acids may have a significant effect.

The main objective of the paper was to present a method for analyzing rainfall-runoff data using geochemical modeling. This approach has scientific merit, and it remains valid regardless of the age of any given data to which it is applied. Although the only available data sets happen to be 35 years old, this does not preclude conducting the same type of study under current environmental conditions. In fact, one of the major findings of this analysis is the relative importance of non-acidic deposition components, presumably organic acids, in the attack on marble and bronze. These components have become even more important because rain acidity and ambient levels of SO_2 have been declining, at least in Western Europe and N. America. Consequently, there is a current need for such mass balance studies in these regions in order to gain a better understanding of the effects of these organic acids, and particularly the anthropogenic contribution to them.

For other parts of the world such as China and India, where levels of both acidic and non-acidic air pollutants are increasing, there is growing concern about the protection of cultural heritage (Price and Doehne, 2010) Effective air pollution management strategies to achieve this protection will require an accurate assessment of the relative importance of the individual components of materials damage. However, not enough monitoring data are available to make any assessments of deposition levels (Vet et al., 2014). The mass balance method has the potential of identifying the dominant agents of deterioration at a given site at relatively low cost.

This would involve exposing standardized specimens of carbonate stone and patinated copper or bronze with associated rain and runoff collectors. The analytes should include for the stone: pH, conductivity, sulfate, nitrate, ammonia, chlorine, calcium, magnesium, potassium, sodium and organic acids. For bronze, copper, zinc, tin and lead should also be included.

References

Albrecht, T., Addai-Mensah, J., Fornasiero, D., 2011. Effect of Temperature on Copper and Zinc Hydroxide Formation/Precipitation, Chemeca 2011 (Sydney, Australia).
Aloiz, E., Grissom, C., Davis, J.M., Livingston, R.A., 2012. Characterization of the Smithsonian Institution's building stones using conventional and advanced analytical methods. In: Wheeler, G. (Ed.), 12th International Congress on the Deterioration and Conservation of Stone. Columbia University.
ASTM, 2011. ASTM G1–03(2011): Standard Practice for Preparing, Cleaning, and Evaluating Corrosion Test Specimens. ASTM International, West Conshohocken, PA.
Baboian, R., Cliver, E.B., 1986. Corrosion on the Statue of Liberty:Part four-copper behavior. Mater. Perform. 25, 80–83.
Bardouki, H., Liakakou, H., Economou, C., Sciare, J., Smolk, J., Zdmal, V., Eleftheriadis, K., Lazaridis, M., Dye, C., Mihalopoulos, N., 2003. Chemical composition of size-resolved atmospheric aerosols in the eastern Mediterranean during summer and winter. Atmos. Environ. 37, 195–208, 114.
Bassett, H., Durrant, R.G., 1922. CCCXVII.-Action of ammonium nitrate and of aqueous ammonia on copper. Properties of cupric tetrammine nitrite and nitrate. J. Chem. Soc. Trans. 121, 2630–2640.
Butler, J., 1982. Carbon Dioxide Equilibria and Their Applications. Addison-Wesley, Reading MA.
Camuffo, D., Del Monte, M., Sabbioni, C., Vittori, O., 1982. Wetting, deterioration and visual features of stone surfaces in an urban area. Atmos. Environ. 16, 2253–2259.
Cardell-Fernandez, C., Vleugels, G., Torfs, K., Van Grieken, R., 2002. The processes dominating Ca dissolution of limestone when exposed to ambient atmospheric conditions as determined by comparing dissolution models. Environ. Geol. 43, 160–171.
CDA, 2015. Copper in Architecture – Design Handbook. Copper Development

Association, New York, NY.
Chebbi, A., Carlier, P., 1996. Carboxylic acids in the troposphere, occurrence, sources, and sinks: A Review. Atmos. Environ. 30, 4233–4249.
Davidson, C.I., Tang, W., Finger, S., Etymezian, V., Striegel, M.F., Sherwood, S.I., 2000. Soiling patterns on a tall limestone building: changes over 60 years. Environ. Sci. Technol. 34, 560–565.
Delaware, R., 1982. Personal Communication. New York State Dept. of Environmental Conservation.
Drewnick, F., Jayne, J.T., Canagaratna, M., Worsnop, D.R., Demerjian, K.L., 2004. Measurement of ambient aerosol composition during the PMTACS-NY 2001 using an aerosol mass spectrometer. Part II: chemically speciated mass distributions. Aerosol Sci. Technol. 38, 104–117.
Evans, M.C.F., 2003. Characterization and Formation of Particulate Nitrate in a Coastal Area, (unpublished Ph.D. dissertation), Chemistry Dept. University of South Florida, Tampa, FL.
Ferrand, E., Blade, E.F., 1969. Sulfur dioxide pollution in New York City: statistical analysis of twelve years. JAPCA 19, 873–878.
Ford, D., Williams, P.D., 2007. Karst Hydrogeology and Geomorphology. Revised Edition. John Wiley & Sons Ltd., Chicester, UK.
Hughes, R., Rowes, M., 1991. The Colouring, Bronzing and Patination of Metals: a Manual for Fine Metalworkers, Sculptors and Designers, second ed. Thames and Hudson, London.
Kratschmer, A., Odnevall Wallinder, I., Leygraf, C., 2002. The evolution of outdoor copper patina. Corros. Sci. 44, 425–450.
Livingston, R.A., 1986. Evaluation of building deterioration rates by water runoff. In: Davis, G. (Ed.), Building Performance: Function, Preservation and Rehabilitation, STP 901. American Society for Testing and Materials, Philadelphia, PA, pp. 181–188.
Livingston, R.A., 1991. The influence of the environment on the patina of the Statue of Liberty. Env. Sci. Technol. 25, 1401–1407.
Livingston, R.A., Kantz, M., Dorsheimer, J., 1982. Stone Deterioration at Bowling Green Custom House 1980-81: Interim Report. EPA 600/6-84-003, Springfield VA.
Lobnig, R.E., Frankenthal, R.P., Siconolfi, D.J., Sinclair, J.D., Stratmann, M., 1994. Mechanism of atmospheric corrosion of copper in the presence of submicron ammonium sulfate particles at 300 and 373 K. J. Electrochem. Soc. 141, 2935–2941.
Lobnig, R.E., Jankoski, C.A., 1998. Atmospheric corrosion of copper in the presence of acid ammonium sulfate particles. J. Electrochem. Soc. 145, 946–956.
Meakin, J.D., Ames, D.L., Dolske, D.A., 1992. Degradation of monumental bronzes. Atmos. Environ. 26B, 207–212.
Mossotti, V.G., Eldeeb, A.R., Reddy, M.M., Fries, T.L., Coombs, M.J., Schmiermund, R.L., Sherwood, S.I., 2001. Statistical Compilation of NAPAP Chemical Erosion Observations. Open File Report 98–755. U.S. Geological Survey, Reston, VA.
Moussiopoulos, N., Sahm, P., Kessler, C., 1995. Numerical simulation of photochemical smog formation in athens, Greece-A case study. Atmos. Environ. 29, 3619–3632.
NADP, 2014. National Trends Network Annual Maps. NADP Program Office, Illinois State Water Survey, Champaign, IL. http://nadp.sws.uiuc.edu/ntn/maps.aspx (accessed 17.08.16.).
NOAA, 2015. U.S. Climate Atlas. NOAA National Centers for Environmental Information, Asheville, NC. http://www1.ncdc.noaa.gov/pub/data/images/olstore/SelClimMapsPubOnlineReduced_3.pdf (accessed 19.08.16.).
NYDEC, 2012. 2011 Region 2 Air Quality Data. New York State Department of Conservation. http://www.dec.ny.gov/airmon/ (accessed 19.08.16.).
O' Brien, P.F., Bell, E., Orr, T.L.L., Cooper, T.P., 1995. Stone loss rates at sites around Europe. Sci. Total Environ. 167, 111–121.
Price, C.A., Doehne, E., 2010. Stone Conservation: An Overview of Current Research, Second ed. Getty Conservation Institute, Los Angeles.
Rockwell International, 1982. Operations and Maintenance Manual for Precipitation Chemistry Measurement Systems, EPA 600/4-82-042 a+b. Environmental Protection Agency, Research Triangle Park, NC.
Roth, B., Okada, K., 1998. On the modification of sea-salt particles in the coastal atmosphere – a TEM study. Atmos. Environ. 32, 1555–1569.
Selwyn, L.S., 1996. Outdoor bronze statues: analysis of metal and surface samples. Stud. Conserv. 41, 205–228.
Shapiro, J.P., 2007. Precipitation chloride at West Point, NY: Seasonal patterns and possible contributions from non-seawater sources. Atmos. Environ. 41, 2240–2254.
Smithsonian American Art Museum, 2015. Save Outdoor Sculpture Database. http://americanart.si.edu/research/programs/sos/ (accessed 19.08.16.).
Souza, S.R., Vasconcellos, P.C., Carvalho, L.R.F., 1999. Low molecular weight carboxylic acids in an urban atmosphere: winter measurements in Sao Paulo City, Brazil. Atmos. Environ. 33, 2563–2574.
Steiger, M., 2015. Air pollution damage to stone. In: Brimblecombe, P. (Ed.), Urban Pollution and Changes to Materials and Building Surfaces. Imperial College Press, pp. 65–102.
Stephenson, W.J., Finlayson, B.L., 2009. Measuring erosion with the micro-erosion meter—Contributions to understanding landform evolution. Earth Sci. Rev. 95, 53–62.
Stumm, W., Morgan, J.J., 1981. Aquatic Chemistry: an Introduction Emphasizing Chemical Equilibria in Natural Waters. John Wiley & Sons, New York.
Tidblad, J., 2015. Air pollution damage to metals. In: Brimblecombe, P. (Ed.), Urban Pollution and Changes to Materials and Building Surfaces. Imperial College Press, pp. 143–164.
Vet, R., Artz, R.S., Carou, S., Shaw, M., Ro, C.-U., Aas, W., Baker, A., Bowersox, V.C., Dentener, F., Galy-Lacaux, C., Hou, A., Pienaar, J.J., Gillett, R., Forti, M.C., Gromov, S., Hara, H., Khodzher, T., Mahowald, N.M., Nickovic, S., Rao, P.S.P., Reid, N.W., 2014. A global assessment of precipitation chemistry and deposition of sulfur, nitrogen, sea salt, base cations, organic acids, acidity and pH, and phosphorus. Atmos. Environ. 93, 3–100.
Winkler, E.M., 1973. Stone in Architecture: Properties, Durability, Second ed. Springer-Verlag, New York.
Wu, Y.L., Davidson, C.I., Dolske, D.A., Sherwood, S.I., 1992. Dry deposition of atmospheric contaminants: the relative importance of aerodynamic, boundary layer, and surface resistances. Aerosol Sci. Technol. 16, 65–81.
Zhang, X., He, W., Odnevall Wallinder, I., Pan, J., Leygraf, C., 2002. Determination of instantaneous corrosion rates and runoff rates of copper from naturally patinated copper during continuous rain events. Corros. Sci. 44, 2131–2151.
Zhuang, H., Chan, C.K., Fang, M., Wexler, A.S., 1999. Formation of nitrate and non-sea-salt sulfate on coarse particles. Atmos. Environ. 33, 4223–4233.